

Article

Electrical, Structural, Optical, and Adhesive Characteristics of Aluminum-Doped Tin Oxide Thin Films for Transparent Flexible Thin-Film Transistor Applications

Seung-Hun Lee ^{1,2}, Kihwan Kwon ^{1,3}, Kwanoh Kim ¹, Jae Sung Yoon ^{1,4}, Doo-Sun Choi ¹, Yeongeun Yoo ^{1,4}, Chunjoong Kim ², Shinill Kang ^{3,*} and Jeong Hwan Kim ^{1,4,*}

¹ Department of Nano Manufacturing Technology, Korea Institute of Machinery and Materials (KIMM), Daejeon 34103, Korea; qwpo45ei@kimm.re.kr (S.-H.L.); nankkh@kimm.re.kr (K.K.); kkim@kimm.re.kr (K.K.); jaesyoon@kimm.re.kr (J.S.Y.); choids@kimm.re.kr (D.-S.C.); yeyoo@kimm.re.kr (Y.Y.)

² Department of Materials Science and Engineering, Chungnam National University, Daejeon 34134, Korea; ckim0218@cnu.ac.kr

³ School of Mechanical Engineering, Yonsei University, Seoul 03722, Korea

⁴ Department of Nano-Mechatronics, University of Science and Technology, Daejeon 34113, Korea

* Correspondence: snlkang@yonsei.ac.kr (S.K.); jkim@kimm.re.kr (J.H.K.)

Received: 6 November 2018; Accepted: 29 December 2018; Published: 3 January 2019



Abstract: The properties of Al-doped SnO_x films deposited via reactive co-sputtering were examined in terms of their potential applications for the fabrication of transparent and flexible electronic devices. Al 2.2-atom %-doped SnO_x thin-film transistors (TFTs) exhibit improved semiconductor characteristics compared to non-doped films, with a lower sub-threshold swing of ~ 0.68 Vdec⁻¹, increased on/off current ratio of $\sim 8 \times 10^7$, threshold voltage (V_{th}) near 0 V, and markedly reduced (by 81%) V_{th} instability in air, attributable to the decrease in oxygen vacancy defects induced by the strong oxidizing potential of Al. Al-doped SnO_x films maintain amorphous crystallinity, an optical transmittance of $\sim 97\%$, and an adhesive strength (to a plastic substrate) of over 0.7 kgf/mm; such films are thus promising semiconductor candidates for fabrication of transparent flexible TFTs.

Keywords: thin-film transistor; tin oxide; aluminum doping; oxide semiconductor; adhesive property

1. Introduction

In recent years, intensive research efforts have focused on metal oxide semiconductors, such as ZnO, SnO₂, In₂O₅, and InGaZnO₅, which have many applications in electronics, sensors, and active matrix displays. Because of their high electron mobility and good transparency, metal oxide semiconductors are especially ideal candidates for the active layers of thin-film transistors (TFTs) [1–7]. Most metal oxide semiconductors are fabricated via sputtering; their properties are determined by reactions between the injected gases (Ar and O₂) and the metals (e.g., In, Sn, Zn, and Ga), typically yielding amorphous, conductive, and transparent materials. Especially compared to amorphous silicon, metal oxide semiconductors can be fabricated at a relatively low temperature (≤ 300 °C), even room temperature, and have higher electron mobility than amorphous silicon, thus finding many applications in the manufacture of organic light-emitting diode display panels.

However, metal oxide semiconductors have a problem of stability, because of oxygen deficiencies and reaction with the external environment. The high electron carrier level caused by oxygen vacancies also compromises semiconductor device controllability. Therefore, it is very important to reduce oxygen vacancy defects. If a doped component could maintain the oxygen content in the metal oxide semiconductors, the device stability and controllability would improve [8].

Here, we fabricated Al-doped SnO_x films via sputtering and explored the effect of the Al doping on SnO_x films on electrical, structural, and optical properties. We further fabricated TFTs to investigate their transfer characteristics and stability. In addition, we used a simple peel test to estimate adhesion between Al-doped SnO_x thin films and flexible plastic substrates at different Al contents, which would be critical to flexible device fabrication [9–11].

2. Materials and Methods

Bottom gate TFTs based on Al-doped SnO_x were fabricated. Highly doped Si (P⁺⁺) and thermally grown SiO₂ (100 nm) served as the gate electrode and insulator, respectively. As a channel layer, 10 nm thick SnO₂ films were deposited using radiofrequency (RF) reactive magnetron sputtering. For Al doping of SnO₂, co-sputtering was performed using Sn (99.999%) and Al (99.999%) targets and an O₂/Ar gas mixture (O₂:Ar = 1:3). To explore the effects of doping, the input RF power of the Al target was varied from 0 to 100 and 200 W (yielding TFTs termed SO, ASO1, and ASO2, respectively), whereas that of the Sn target was fixed at 200 W. The channel thickness of all three samples was fixed at 10 nm, as confirmed using a spectroscopic ellipsometer (MG-1000, Nano-View Co., Ansan, Korea) and a field effect scanning electron microscope (S5300, Hitachi Inc., Tokyo, Japan). The source/drain electrodes were 10 wt % Sn-doped In₂O₃ (indium tin oxide), deposited via direct-current magnetron sputtering at 200 W to a thickness of 100 nm. 1000 μm wide and 100 μm long channel patterns were created using a shadow mask. Sputtering was performed at a base pressure of 1 × 10^{−6} Torr and a working pressure of 10 mTorr at room temperature. The TFTs were subjected to thermal annealing at 150 °C for 1 h in air using a quartz tube furnace. The electrical performance of the Al-doped SnO_x TFTs was measured using an HP4145B semiconductor analyzer operating at room temperature in the dark. In addition, we measured changes in TFT transfer characteristics over time. TFTs without passivation layers were exposed to the air at room temperature under dehumidifying condition. The chemical compositions and Sn-bonding states of the Al-doped SnO_x thin films were analyzed by X-ray photoelectron spectroscopy (XPS) (Multilab 2000, Thermo Scientific Ltd., Waltham, MA, USA). The atomic percentage of each element in the films was calculated by dividing the area under the curve by the relative sensitivity factor for each peak at C 1s, Al 2p, Sn 3d, and O 1s XPS spectra and normalizing the values over the total amount of the elements in the films. Carrier densities were measured using the Hall method (HMS-5300, Ecopia, Anyang, Korea), employing the Van der Pauw configuration. Crystallinity was evaluated via high-resolution X-ray diffraction (HR-XRD), during which Cu Kα radiation was delivered at a glancing angle (D8 Discover, Bruker AXS Ltd., Karlsruhe, Germany). Optical transmittance was assessed with the aid of a UV-visible spectrophotometer (UV-2450, Shimadzu Corp., Tokyo, Japan). A peel tester stand (AD4935-50N, And Inc., Tokyo, Japan) and duct tape (GT2, 3M Espe, Maplewood, NJ, USA) were used to measure adhesion between the Al-doped SnO_x thin films and the polyimide (PI) films. Samples were fixed to glass to prevent cracking during bending or handling. Changes in sheet resistance after the peel test were analyzed via four-point probing using a source meter (2400, Keithley Inc., Beaverton, AL, USA) to evaluate adhesion between the Al-doped SnO_x thin films and the PI films.

3. Results and Discussions

3.1. Electrical Characterization of Al-Doped SnO_x Thin-Film Transistors

Figure 1 shows the transfer characteristics of SO, ASO1, and ASO2, which were scanned with forward (−20 V → +20 V) and reverse (+20 V → −20 V) bias sweeps. The source and drain voltages (V_D) were the constant ground voltage and 10.1 V, respectively. The threshold voltage (V_{th}) was the voltage evident when the current approached L/W × 10 nA [12]. The saturation mobility (μ_{sat}) and subthreshold swing (SS) were 2L/WC_i × (dI_D^{1/2}/dV_G)² and (dlog I_D/dV_G)^{−1} respectively, where C_i is the capacitance per unit area of the gate dielectric (34.5 nF/cm²) [13–15]. The V_{th}, I_{on}/I_{off}, μ_{sat}, SS, and Al atomic concentrations (in atom %) of SO, ASO1, and ASO2 are listed in Table 1. The Al atomic

percentage values were evaluated via XPS spectral analysis, assuming that the films consisted of C, Al, Sn, and O. As shown in Figure 1, the TFT device exhibited n-type conduction. Although SnO₂ is a well-known n-type material, several papers have reported that Al-incorporated SnO_x showed p-type semiconducting behavior. This is due to the hole carriers produced by the Al³⁺-Sn⁴⁺ substitution reaction when the Al concentration exceeds 5% in a SnO₂ film [16,17]. Therefore, it is possible the n-type behavior of the TFT may be caused by the low concentration ($\leq 2.24\%$) of Al, which is not enough to make holes majority carriers in SnO_x films. As the extent of Al doping increased, V_{th} changed from -13.4 to -1.0 V, thus becoming close to 0 V, and the I_{on}/I_{off} ratio increased dramatically (over 25-fold) because the off-current was much lower than that of undoped SnO_x. Chu et al. reported that reduced carrier concentration in the n-type channel material induces higher V_{th} and lower I_{off} , because the channel with lower carrier concentration is more easily depleted [18]. Therefore, these positive shifts of V_{th} and decreased I_{off} are attributable to reductions in electron density in the TFT channels as Al levels increase [2,6,18,19]. In general, oxygen vacancies in SnO_x-based materials generate free electrons, which is accompanied by n-type semiconduction [20,21]. The standard oxidation potential (at 25 °C) of Al is higher than that of Sn by 1.37 V; Al is thus a stronger oxidizer than Sn [22]. Hence, if enough oxygen is supplied during the sputtering process, fewer oxygen vacancies are induced in Al-doped SnO_x layers compared to non-doped SnO_x, because the film oxygen content is higher given the stronger oxidizing power of Al. Consequently, decreasing electron density with increasing Al content in the film could be attributed to fewer oxygen vacancies in the ASO1 and ASO2 channels due to the strong oxidizing potential of Al, resulting in the increased V_{th} and I_{on}/I_{off} ratio. Moreover, the insulating property of Al₂O₃, which was formed during the RF sputtering process in the Ar/O₂ ambience, could be another reason for lower electron density compared to non-doped SnO_x layer. Hall measurements confirmed the reductions in electron density, which were $9.41 \times 10^{18} \text{ cm}^{-3}$ for SO and $6.09 \times 10^{15} \text{ cm}^{-3}$ for ASO2. The μ_{sat} ($2.27 \pm 0.03 \text{ cm}^2 \text{ V}^{-1} \text{ s}^{-1}$) did not change significantly after doping, which was also confirmed by the similar slope in Figure S1 in the supplementary material. However, the SS of ASO2 fell to 0.68 V dec.^{-1} , less than 33% of that of SO, further improving TFT performance. Clockwise hysteresis was observed, and revealed that electron traps existed at or near the channel/insulator interface. The hysteresis ($|\Delta V_{th}|$) of ASO2 was decreased to 1.13 V, much less than that of SO (2.67 V), which indicates that the hysteresis can be obviously suppressed by Al doping.

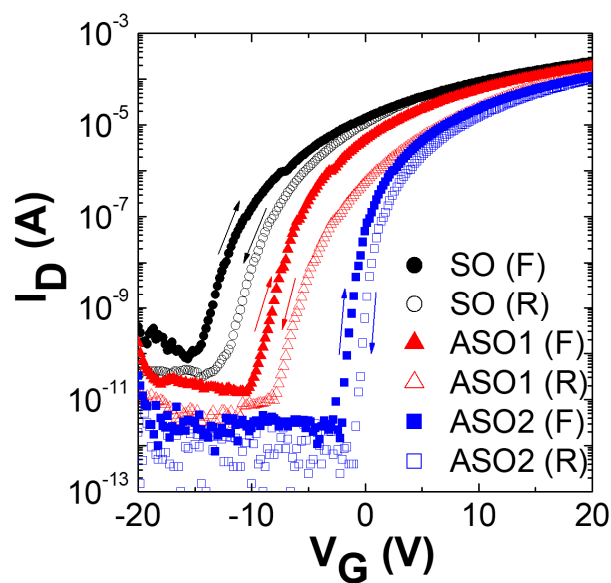


Figure 1. Transfer curves of the SO, ASO1 and ASO2 thin-film transistors (TFTs) containing Al at atom % values of 0, 1.20, and 2.24, which were scanned with forward (F) and reverse (R) bias sweeps ($V_D = 10.1$ V).

Table 1. Electrical parameters revealed by the thin-film transistor (TFT) transfer curves scanned with forward bias sweep, hysteresis (H) in clockwise direction and Al atomic concentrations from X-ray photoemission spectroscopy (XPS) spectral analyses.

Sample	V_{th} [V]	I_{on}/I_{off}	μ_{sat} [$cm^2 V^{-1} s^{-1}$]	SS [V dec $^{-1}$]	H [V]	Al [at %]
SO	−13.4	3.11×10^6	2.24	2.37	2.67	0
ASO1	−8.0	1.38×10^7	2.30	1.28	2.15	1.20
ASO2	−1.0	7.86×10^7	2.24	0.68	1.13	2.24

We explored changes in TFT transfer characteristics over time (Figure 2). V_G - I_D curves were drawn daily for 2 weeks after TFT fabrication; the V_{th} values gradually became more positive because the channels absorbed atmospheric oxygen [23,24]. After 14 days, the V_{th} values of SO, ASO1, and ASO2 had shifted by 6.2, 4.2, and 1.2 V, respectively, indicating that the ambient stability of SnO_x film can be improved by Al doping. Yan et al. reported that oxygen adsorption is preferred on oxygen-deficient surfaces, and that molecular oxygen can heal oxygen vacancies in the oxide material [25]. Therefore, this decreased V_{th} shift with increasing Al content is attributable to the reduced reaction between the surfaces of the channels and the oxygen in the atmosphere, because Al-doped channels have fewer oxygen vacancies than undoped channels, as discussed in Figure 1.

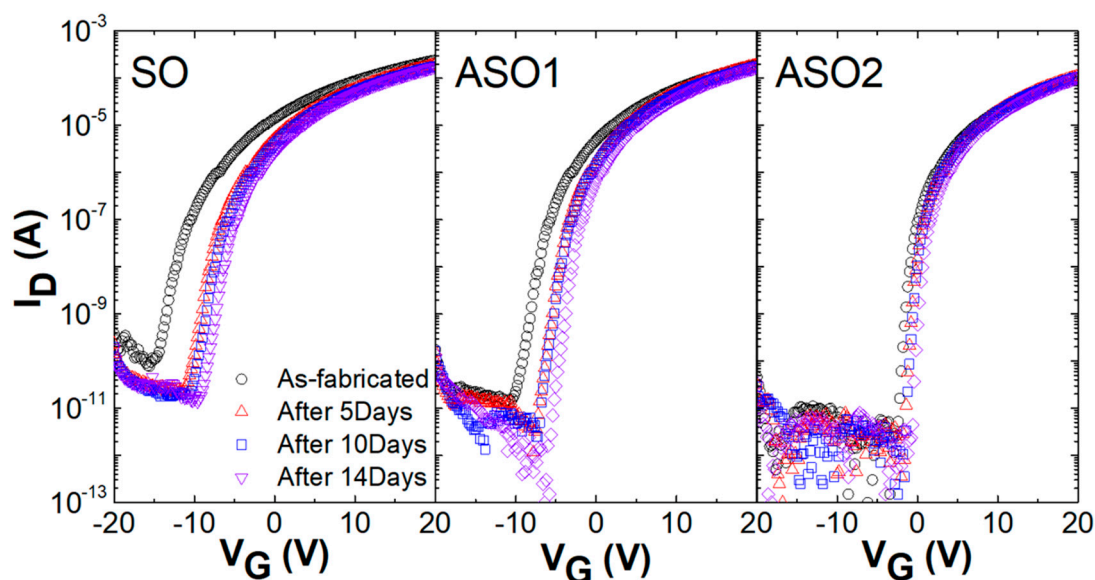


Figure 2. Changes in the transfer characteristics of SO, ASO1, and ASO2 TFTs (lacking passivation layers) over time.

3.2. Structural and Optical Properties of Al-Doped SnO_x Thin-Films

In order to support the electrical characteristics of the TFTs, we performed analyses of structural and optical properties of SnO_x thin films with different Al concentrations. Figure 3a shows the Sn $3d_{5/2}$ XPS spectra of the SO, SAO1, and SAO2 films. The Sn $3d_{5/2}$ peaks were deconvoluted into two sub-peaks with binding energies of 487.0 and 486.3 eV [19,26], respectively, corresponding to the Sn^{4+} and Sn^{2+} binding states. The Sn^{2+} peak area clearly decreased with the Al proportion, while that of the Sn^{4+} peak increased. The relative peak intensity [$Sn^{2+}/(Sn^{2+} + Sn^{4+})$] of the Sn^{2+} peak fell from 0.37 to 0.16 with increasing Al doping (Figure 3b). Huh et al. found that Sn^{2+} binding in SnO_2 caused oxygen vacancy defects [19]. Moreover, the O 1s peaks were deconvoluted into two sub-peaks corresponding to the lattice oxygen (O_L) and oxygen deficiency (O_D), located at 530.9 and 531.3 eV [2,27] respectively, as shown in Figure 3c. As the Al doping increases, the reduction of O_D peak area can be evidently observed, as confirmed in Figure 3d, which shows the decrease of the relative peak intensity [$O_D/(O_L + O_D)$] of O_D peak from 0.22 to 0.18 with increasing Al concentration.

Therefore, the reductions in the proportions of the Sn^{2+} and O_D peaks with Al content reflect the reductions in electron density and oxygen vacancies; the channels operate efficiently at increasingly higher $I_{\text{on}}/I_{\text{off}}$ ratios and reduced SS, and are more stable in air (see also Figures 1 and 2).

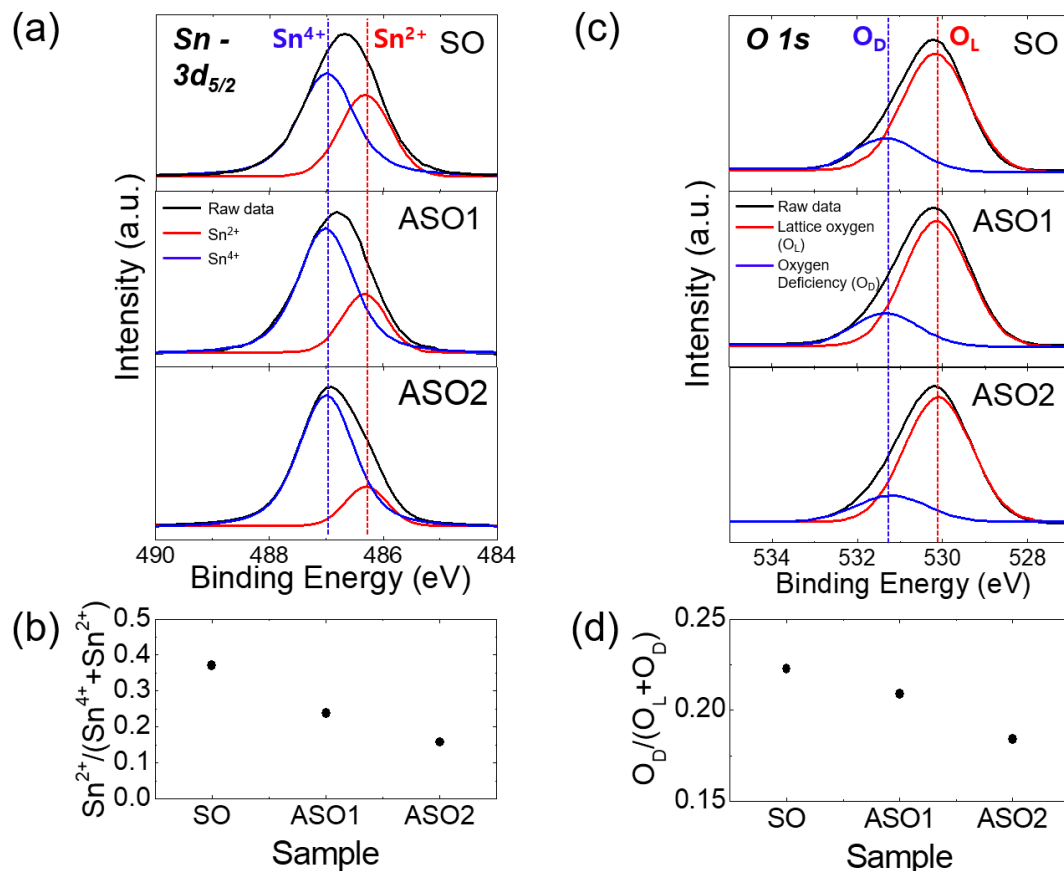


Figure 3. (a) Sn 3d_{5/2} X-ray photoemission spectroscopy (XPS) spectra of SO, ASO1, and ASO2 thin-films. (b) Relative peak intensities [Sn²⁺/Sn⁴⁺ + Sn²⁺] of the Sn²⁺ peaks. (c) O 1s XPS spectra of SO, ASO1, and ASO2 thin films. (d) Relative peak intensities of [O_D/(O_L + O_D)] of the O_D peaks.

Next, SO, ASO1, and ASO2 thin films formed on Si/SiO₂ (100 nm) substrates were subjected to glancing-angle HR-XRD to evaluate crystallinity changes (Figure 4). The samples were prepared with the thickness of 20 nm to ensure that, if present, diffraction peaks would be evident, and annealed at 150 °C for 1 h. All samples were amorphous, lacking the diffraction peaks identified earlier [19,28]. This means our films have high areal uniformity for device characteristics, which is essential for fabricating devices on large-scale substrate [1]. To evaluate optical properties, 10 nm thick films were deposited on glass. As shown in Figure 5, all visible ($\lambda = 390\sim 700$ nm) optical transmittances were >97%, and optical band-gaps determined by extrapolating the best fit to the intercept (at $\alpha = 0$) in the Tauc plot [2,29] were ~ 3.5 eV plot for all samples, as required for fabrication of transparent electronic devices.

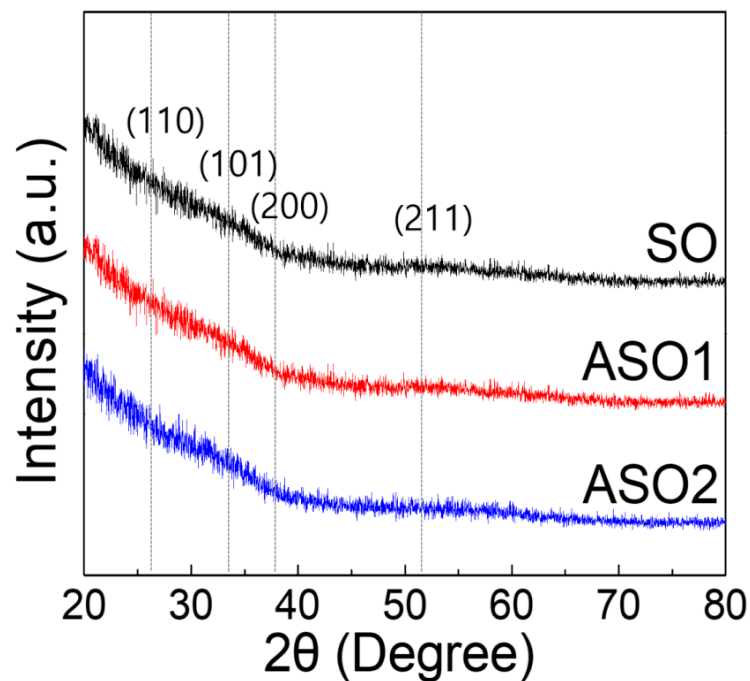


Figure 4. High resolution X-ray diffraction (HR-XRD) patterns of SO, ASO1, and ASO2 thin-films with different Al concentrations.

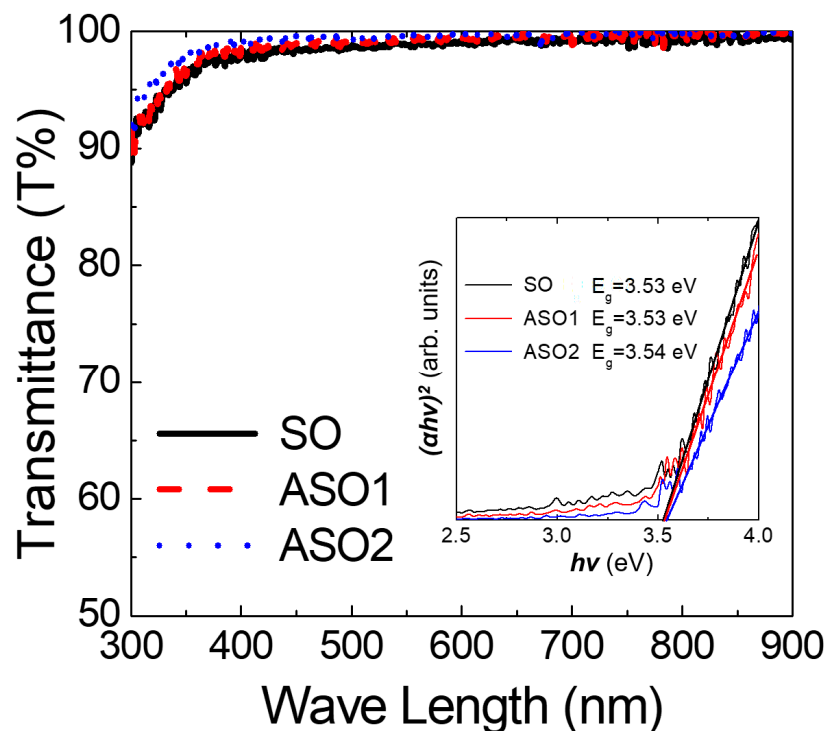


Figure 5. Optical transmittance values as a function of wavelength and (inset) Tauc plot as a function of photon energy ($h\nu$) for the SO, ASO1, ASO2 thin films with different Al concentrations.

3.3. Adhesive Property between Al-Doped SnO_x Thin-Films and Plastic Substrate

We used the peel test to investigate the adhesion between the Al-doped SnO_x thin-films and PI substrates that are known to be stable below 260 °C. 10 nm thick SO, ASO1, and ASO2 thin films were RF-sputtered onto pre-cleaned PI and annealed at 150 °C. The peel test was performed using duct tape

with an adhesion strength ≥ 0.7 kgf/mm (as revealed by a 180° peel test using the samples and the tape). The tape remained perfectly bonded to the SO, ASO1, and ASO2 surfaces under a vertical load of 5 kg, and was then detached. Figure 6 shows the sheet resistance values before and after the peel test. For the SO, ASO1 and ASO2 films, these were ~ 177 , ~ 4613 and $\sim 89,742$ k Ω /sq. prior to the peel test, respectively. The sheet resistance of fabricated samples gradually increased with increasing Al content, attributable to the decreased carrier concentrations and improved semiconductor characteristics (see Figure 1). No significant change was evident after the peel test. If peeling occurred at the interface between a thin film and the polymer substrate, the film sheet resistance would increase. Although we did not measure the maximal adhesive strength, this was >0.7 kgf/mm, thus above the adhesive strength of duct tape.

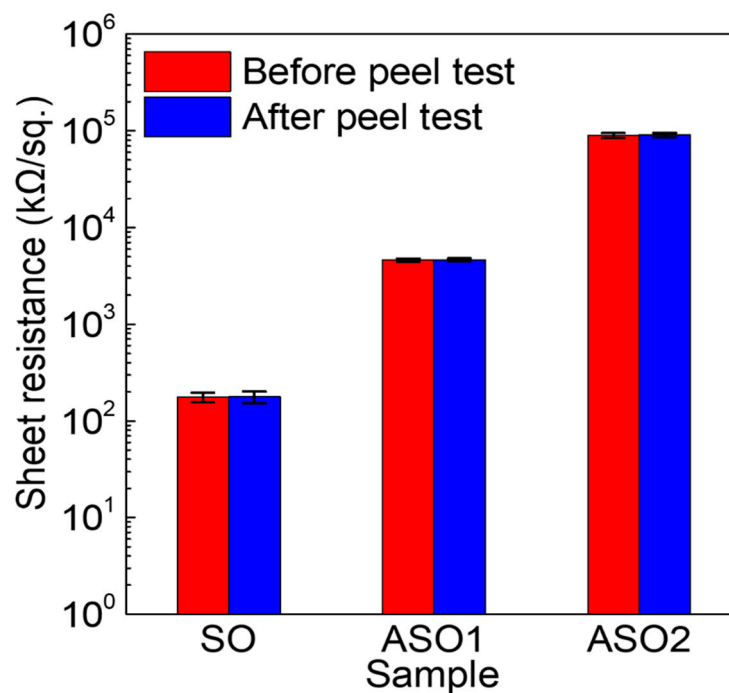


Figure 6. Sheet resistance changes before and after the peel test for SO, ASO1, and ASO2 thin films on a polyimide (PI) substrate.

4. Conclusions

We fabricated SnO_x-based TFTs doped with different levels of Al via RF reactive co-sputtering. Compared to SnO_x, the Al-doped films exhibited improved channel semiconductor characteristics, including a shift in V_{th} to almost 0 V, an increased I_{on}/I_{off} ratio, a reduced SS, and improved stability in air, which are attributable to the reduced oxygen deficiencies (because Al is a stronger oxidizer than Sn). The oxygen deficiency reduction by Al doping was confirmed by the decrease of Sn²⁺ and O_D proportion in Sn 3d_{5/2} and O 1s XPS spectral analysis. The Al-doped SnO_x films are amorphous and have an optical transmittance of $\sim 97\%$ and an adhesive strength (to PI) of >0.7 kgf/mm, which facilitates their use in flexible and transparent electronics.

Supplementary Materials: The following are available online at <http://www.mdpi.com/1996-1944/12/1/137/s1>, Figure S1: The $(I_{DS})^{1/2}$ versus V_G curves of SO, ASO1, and ASO2 TFTs for comparison of electron mobilities at $V_D = 10.1V$.

Author Contributions: S.-H.L., K.K. (Kihwan Kwon), Y.Y., S.K. and J.H.K. conceived and designed the experiments; S.-H.L. and J.H.K. performed the experiments; S.-H.L., K.K. (Kihwan Kwon), K.K. (Kwanoh Kim), J.S.Y., Y.Y., C.K., S.K. and J.H.K. analyzed the data; D.-S.C., Y.Y. contributed materials/analysis tools; S.-H.L. prepared original draft; J.H.K. revised the manuscript.

Funding: The research was supported by a National Research Foundation of Korea (NRF) grant funded by the Ministry of Science and ICT for the First-Mover Program for Accelerating Disruptive Technology Development (NRF-2018M3C1B9069841). The work was also funded by Korea Institute of Machinery and Materials (NK211D).

Conflicts of Interest: The authors declare no conflict of interest.

References

1. Nomura, K.; Ohta, H.; Takagi, A.; Kamiya, T.; Hirano, M.; Hosono, H. Room-temperature fabrication of transparent flexible thin-film transistors using amorphous oxide semiconductors. *Nature* **2004**, *432*, 488–492. [[CrossRef](#)] [[PubMed](#)]
2. Kim, J.I.; Ji, K.H.; Jang, M.; Yang, H.; Choi, R.; Jeong, J.K. Ti-doped indium tin oxide thin films for transparent field-effect transistors: Control of charge-carrier density and crystalline structure. *ACS Appl. Mater. Interfaces* **2011**, *3*, 2522–2528. [[CrossRef](#)]
3. Fortunato, E.M.C.; Barquinha, P.M.C.; Pimentel, A.C.M.B.G.; Concalves, A.M.F.; Marques, A.J.S.; Pereira, L.M.N.; Martins, R.F.P. Fully Transparent ZnO thin-film transistor produced at room temperature. *Adv. Mater.* **2005**, *17*, 590–594. [[CrossRef](#)]
4. Maiolo, L.; Mirabella, S.; Maita, F.; Alberti, A.; Minotti, A.; Strano, V.; Pecora, A.; Shacham-Diamand, Y.; Fortunato, G. Flexible pH sensors based on polysilicon thin film transistor and ZnO nanowalls. *Appl. Phys. Lett.* **2014**, *105*, 093501. [[CrossRef](#)]
5. Kim, H.Y.; Jung, E.A.; Mun, G.; Agbenteke, R.E.; Park, B.K.; Park, J.S.; Son, S.U.; Jeon, D.J.; Park, S.H.K.; Chang, T.M.; et al. Low-temperature growth of indium oxide thin film by plasma-enhanced atomic layer deposition using liquid dimethyl(N-ethoxy-2,2-dimethylpropanamido)indium for high-mobility thin film transistor application. *ACS Appl. Mater. Interfaces* **2016**, *8*, 26924–26931. [[CrossRef](#)]
6. Sheng, J.; Jeong, H.-J.; Han, K.-L.; Hong, T.H.; Park, J.-S. Review of recent advances in flexible oxide semiconductor thin-film transistors. *J. Inf. Disp.* **2017**, *18*, 159–172. [[CrossRef](#)]
7. Lee, H.; Zhang, X.; Kim, J.W.; Kim, E.-J.; Park, J. Investigation of the Electrical Characteristics of Bilayer ZnO/In₂O₃ Thin-Film Transistors Fabricated by Solution Processing. *Materials* **2018**, *11*, 2013. [[CrossRef](#)]
8. Minami, T.; Miyata, T.; Ohtani, Y.; Kuboi, T. Effect of thickness on the stability of transparent conducting impurity-doped ZnO thin films in a high humidity environment. *Phys. Status Solidi RRL* **2007**, *1*, R31–R33. [[CrossRef](#)]
9. Lewis, J. Material challenge for flexible organic devices. *Mater. Today* **2006**, *9*, 39–45. [[CrossRef](#)]
10. Ramos, M.M.D. Theoretical study of metal-polyimide interfacial properties. *Vacuum* **2002**, *64*, 255–260. [[CrossRef](#)]
11. Hull, T.R.; Colligon, J.S.; Hill, A.E. Measurement of thin film adhesion. *Vacuum* **1987**, *37*, 327–330. [[CrossRef](#)]
12. Lee, C.-K.; Park, S.Y.; Jung, H.Y.; Lee, C.K.; Son, B.-G.; Kim, H.J.; Lee, Y.-J.; Joo, Y.-C.; Jeong, J.K. High performance Zn-Sn-O thin film transistors with Cu Source/drain electrode. *Phys. Status Solidi RRL* **2013**, *7*, 196–198. [[CrossRef](#)]
13. Hamilton, M.C.; Martin, S.; Kanicki, J. Field-effect mobility of organic polymer thin-film transistors. *Chem. Mater.* **2004**, *16*, 4699–4704. [[CrossRef](#)]
14. Li, J.; Ding, X.-W.; Zhang, J.-H.; Zhang, H.; Jiang, W.-Y.; Zhang, Z.-L. Improving electrical performance and bias stability of HfInZnO-TFT with optimizing the channel thickness. *AIP Adv.* **2013**, *3*, 102132. [[CrossRef](#)]
15. Han, S.J.; Kim, S.; Ahn, J.; Jeong, J.K.; Yang, H.; Kim, H.J. Composition-dependent structural and electrical properties of p-type SnO_x thin films prepared by reactive DC magnetron sputtering: Effects of oxygen pressure and heat treatment. *RSC Adv.* **2016**, *6*, 71757–71766. [[CrossRef](#)]
16. Lee, P.-M.; Liu, Y.-S.; Villamagua, L.; Stashans, A.; Carini, M.; Liu, C.-Y. Experimental observation and computer simulation of Al/Sn substitution in p-type aluminum nitride-doped tin oxide thin film. *J. Phys. Chem. C* **2016**, *120*, 4211–4218. [[CrossRef](#)]
17. Ahmed, S.F.; Khan, S.; Ghosh, P.K.; Mitra, M.K.; Chattopadhyay, K.K. Effect of Al doping on the conductivity type inversion and electro-optical properties of SnO₂ thin films synthesized by sol-gel technique. *J. Sol-Gel Sci. Technol.* **2006**, *39*, 241–247. [[CrossRef](#)]
18. Chu, H.-C.; Shen, Y.-S.; Hsieh, C.-H.; Huang, J.-H.; Wu, Y.-H. Low-voltage operation of ZrO₂-gated n-type thin film transistors based on a channel formed by hybrid phases of SnO and SnO₂. *ACS Appl. Mater. Interfaces* **2015**, *7*, 15129–15137. [[CrossRef](#)]

19. Huh, M.S.; Yang, B.S.; Oh, S.; Yoon, K.; Jeong, J.K.; Hwang, C.S.; Kim, H.J. Improvement in the Performance of Tin Oxide Thin-Film Transistors by Alumina Doping. *Electrochem. Solid-State Lett.* **2009**, *12*, H385–H387. [[CrossRef](#)]
20. Saji, K.J.; Mary, A.P.R. Tin oxide based P and N-type thin film transistors developed by RF sputtering. *ECS J. Solid State Sci. Technol.* **2015**, *4*, Q101–Q104. [[CrossRef](#)]
21. Lee, B.K.; Jung, E.; Kim, S.H.; Moon, D.C.; Lee, S.S.; Park, B.K.; Hwang, J.H.; Chung, T.M.; Kim, C.G.; An, K.S. Physical/chemical properties of tin oxide thin film transistors prepared using plasma-enhanced atomic layer deposition. *Mater. Res. Bull.* **2012**, *47*, 3052–3055. [[CrossRef](#)]
22. Lide, D.R. CRC Handbook of Chemistry and Physics, 87th ed. *J. Am. Chem. Soc.* **2007**, *129*, 724. [[CrossRef](#)]
23. Jeong, J.K. The status and perspectives of metal oxide thin-film transistors for active matrix flexible displays. *Semicond. Sci. Technol.* **2011**, *26*, 034008. [[CrossRef](#)]
24. Chong, E.; Chun, Y.S.; Kim, S.H.; Lee, S.Y. Effect of oxygen on the threshold voltage of a-IGZO TFT. *J. Electr. Eng. Technol.* **2011**, *6*, 539–542. [[CrossRef](#)]
25. Yan, Y.; Al-Jassim, M.M.; Wei, S.-H. Oxygen-vacancy mediated adsorption and reaction of molecular oxygen on the ZnO (10-10) surface. *Phys. Rev. B* **2005**, *72*, 161307. [[CrossRef](#)]
26. Moulder, J.F.; Stickle, W.F.; Sobol, P.E.; Bomben, K.D. *Handbook of X-ray Photoelectron Spectroscopy*, 1st ed.; Perkin-Elmer: Minnesota, MN, USA, 1992; p. 127. ISBN 978-0-96-270262-4.
27. Jaiswar, S.; Mandal, K.D. Evidence of enhanced oxygen vacancy defects inducing ferromagnetism in multiferroic $\text{CaMn}_7\text{O}_{12}$ manganite with sintering time. *J. Phys. Chem. C* **2017**, *121*, 19586–19601. [[CrossRef](#)]
28. Nguyen, A.H.-T.; Nguyen, M.-C.; Choi, J.; Han, S.; Kim, J.; Choi, R. Electrical performance enhancement of p-type tin oxide channel thin film transistor using aluminum doping. *Thin Solid Films* **2017**, *641*, 24–27. [[CrossRef](#)]
29. Wang, B.; Yu, X.; Guo, P.; Huang, W.; Zeng, L.; Zhou, N.; Chi, L.; Bedzyk, M.J.; Chang, R.P.H.; Marks, T.J.; et al. Solution-processed all-oxide transparent high-performance transistors fabricated by spray-combustion synthesis. *Adv. Electron. Mater.* **2016**, *2*, 1500427. [[CrossRef](#)]



© 2019 by the authors. Licensee MDPI, Basel, Switzerland. This article is an open access article distributed under the terms and conditions of the Creative Commons Attribution (CC BY) license (<http://creativecommons.org/licenses/by/4.0/>).